A grand canonical Monte Carlo simulation study of water adsorption on Vycor-like hydrophilic mesoporous silica at different temperatures

2004 J. Phys.: Condens. Matter 16 S5329

(http://iopscience.iop.org/0953-8984/16/45/003)

INSTITUTE OF PHYSICS PUBLISHING JOURNAL OF PHYSICS: CONDENSED MATTER

J. Phys.: Condens. Matter **16** (2004) S5329–S5343 PII: S0953-8984(04)75034-1

A grand canonical Monte Carlo simulation study of water adsorption on Vycor-like hydrophilic mesoporous silica at different temperatures

Joël Puibasset[1] **and Roland J-M Pellenq**[2]

[1] Centre de Recherche sur la Matière Divisée, CNRS et Université d'Orléans, 1b rue de la Férollerie, 45071 Orléans cedex 02, France
[2] Centre de Recherche en Matière Condensée et Nanosciences, CNRS, Campus de Luminy, 13288 Marseille cedex 09, France

E-mail: puibasset@cnrs-orleans.fr and pellenq@crmcn.univ-mrs.fr

Received 15 January 2004
Published 29 October 2004
Online at stacks.iop.org/JPhysCM/16/S5329
doi:10.1088/0953-8984/16/45/003

Abstract

The grand canonical Monte Carlo (GCMC) simulation technique is used to study water adsorption and condensation in a realistic Vycor-like silica mesoporous system at various temperatures. Water–water interactions are described using the SPC model while water–silica interactions are calculated in the framework of the PN-TrAZ model. Thermodynamic quantities (namely water adsorption isotherms and isosteric heat of adsorption curves) have been calculated along with water–water and water–Vycor pair distribution functions. The simulated adsorption isotherm at room temperature compares well with published experimental data. Isosteric heat curves are characteristic of adsorption in a heterogeneous environment. We also show that the BET method for specific surface determination is not valid in the case of water confined in silica mesoporous materials. By analysing water–water and water–Vycor pair correlation functions, we demonstrate the existence of strong distortion compared to bulk water due to the influence of the silica surface. The hydrogen bond is significantly elongated and angle distorted.

1. Introduction

The water–silica system is very important in a wide range of research fields: geophysics, pharmaceutics, industry and environment. Most of the evoked processes, water infiltration, de-pollution, phase separation, catalysis etc, involve nanometric scale physics. This explains the intense theoretical, experimental and simulation activity aiming at getting insight into the nature of water at the silica interface. The thermodynamic, dynamic and structural characteristics are actually expected to differ considerably from bulk ones as interfacial properties dominate the physical processes at work at the mesoscale [1–13].

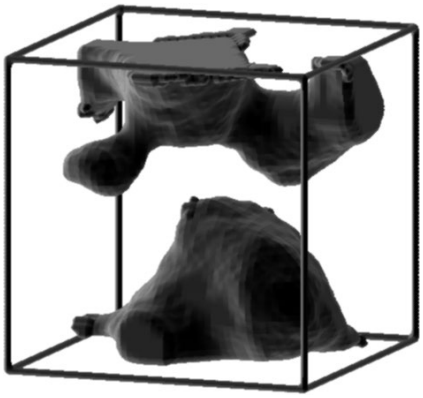

Figure 1. 3D representation of the numerical sample of Vycor used in this study. The porosity is represented in grey. The mean pore size is 36 Å.

The capillary condensation is a striking example of the confinement effect on the thermodynamic properties of a fluid. Structural modifications have also been observed by neutron scattering experiments. For instance, it has been shown that the water structure is distorted in the vicinity of silica surfaces: distortion that may explain why water freezes in cubic ice structure when confined in Vycor, a mesoporous silica glass [14]. More recently, Bruni *et al* [15, 16] have shown how neutron diffraction experiments with isotopic substitution are able to give improved site–site radial distribution functions for water confined in Vycor glass. The results show that water is still hydrogen bonded, but with a distorted network compared to bulk. Molecular dynamics simulation was used to help understand these results. Previous simulation works on water confinement focused on simple silica substrate geometry, slitlike [7, 8] or cylindrical [9, 10] pores, supposed to mimic real porous solids. However, such ideal pores are a rough modelling of real pores, since they introduce only one characteristic pore size and neglect the pore size dispersion and interconnections between pores, or in other words the topology of the system. The present work aims to address both the thermodynamics and the structure of water confined in a realistic mesoporous silica glass, presenting both a morphological (pore size distribution) and a topological (interconnections) disorder. Another originality of this work lies in the statistical ensemble that we explore (grand canonical ensemble) which differs from previous studies of confined water based on molecular dynamics.

2. Description of the mesoporous silica substrate

An off-lattice reconstruction algorithm has been used to generate the atomistic Vycor-like mesoporous structure considered in this study. Portions of an initial cubic crystal of cristobalite (106.95 Å of edge) are cut out by applying the off-lattice functional representing the Gaussian field associated with the volume autocorrelation function of the studied porous structure [17–19]. Periodic boundary conditions are applied to the Gaussian field, so as to generate the periodic structure shown in figure 1. It has been shown [20] that this numerical sample reproduces quite well micro- and meso-textural properties of real Vycor, and constitutes an improvement in the topological description of silica mesoporous glasses, because of the presence of disordered and interconnected pores. To have a realistic description of the surface chemistry, all silicon atoms in an incomplete tetrahedral environment are removed, and all oxygen dangling bonds are saturated with hydrogen atoms placed 1 Å from oxygen perpendicular to the surface. The porosity of the sample is 0.28, the density 1.56 g cm^{-3},

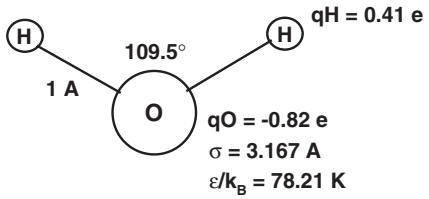

Figure 2. SPC model.

the specific surface area 210 $m^2\ g^{-1}$, the mean pore diameter 36 Å (from chord distribution) and the OH surface density 7 OH nm^{-2}, all in agreement with experimental values: 0.28, 1.50 g cm^{-3}, 200 $m^2\ g^{-1}$ and around 7 OH nm^{-2} if out-gassed around 400 °C [21, 22], except that the pore size is slightly smaller in our pseudo-Vycor compared to the real one (40 Å). It has been shown that this numerical sample reproduces quite well micro and meso textural properties of real Vycor [17–19].

3. Intermolecular potentials

The SPC model [23] has been used to describe the water–water interaction, because it is a fast computable model well suited for very large systems (the completely saturated system contains more than 10 000 water molecules). This model reproduces well the thermodynamic and structural properties around ambient temperature, such as vapour pressure, enthalpy of vaporization [24] and radial distribution functions. In this model, the water molecule is rigid with the geometry defined in figure 2. The molecules interact through electrostatics with the partial charges given in figure 2, and through usual quantum interactions modelled by a Lennard-Jones-like term between the water molecules. Since the main contribution comes from the oxygen atoms, the Lennard-Jones potential is calculated from the oxygen–oxygen distance, and with the parameters given in figure 2.

The interaction of water with Si, O and (surface) H atoms forming the Vycor structure is assumed to remain weak, in the physisorption energy range. In this work, we have used a TrAZ form of the original PN-type potential function as reported for adsorption of rare gases and nitrogen in silicalite-1 [25]. The PN-TrAZ potential function is based on the usual partition of the adsorption intermolecular energy restricted to two-body terms only: it includes a dispersion interaction term, a repulsive short range contribution and an induction term. Three-body dispersion (XYY) terms (where X is the adsorbate and Y an adsorbent species) can be obtained in principle from the same approach [26] but are neglected in the present study since they are only expected to be significant for water molecules in contact with the silica surface (which is a small fraction of the total number adsorbed). The choice of this particular model to describe the water/adsorbent potential was motivated by the good degree of parameter transferability. Indeed, in a previous study [31], we found that, using a set of potential parameters previously derived for adsorption in silica zeolite [25] augmented to take into account hydroxyl groups, the TrAZ model allows reproduction of both the low coverage experimental adsorption isotherm (amount adsorbed *versus* pressure at constant temperature) and isosteric heat curve with no further adjustment. In the TrAZ model, the adsorbate–surface energy ($u^i_{k\in A}$) of the kth atom of molecule A at a position i in the simulation box is given by

$$u^i_{k\in A} = \sum_{j\in\{O,Si,H\}} \left[A_{kj} e^{-b_{kj} r_{ij}} - \sum_{n=3}^{5} f_{2n} \frac{C_{2n,kj}}{r_{ij}^{2n}} \right] - \frac{1}{2}\alpha_k \boldsymbol{E}_i^2 \qquad (1)$$

where r_{ij} is the distance between the matrix species j and the position i of the kth atom of a given molecule, f_{2n} are so-called damping functions that depend on interspecies distance and on a repulsive parameter (see below) and finally $\boldsymbol{E}$ is the electric field created at adsorbate position i due to the inorganic species; all other symbols are physical parameters that depend on electronic properties of interacting species only. The sums runs over all (j) atomic sites in the matrix that are oxygen, silicon and hydrogen atoms. The first term in the sum is a Born–Mayer term representing a two-body form of the short range repulsive energy due to finite compressibility of electron clouds when approaching the adsorbate to very short distance from the pore surface. There is one such term per pair of interacting species. The repulsive parameters (A_{kj} and b_{kj}) are obtained from mixing rules of like-atom pairs (see below). The second term in the above equation is a multipolar expansion series of the dispersion interaction in the spirit of the quantum mechanical perturbation theory applied to intermolecular forces [27]. It has been shown that two- (and three-) body dispersion C_{2n} coefficients for isolated or in-condensed phase species can be obtained from the knowledge of the dipole polarizability and the effective number of polarizable electrons N_{eff} of all interacting species [25, 26] which are closely related to partial charges that can be obtained from *ab initio* calculations. The f_{2n} terms in the above equation are damping functions of the form

$$f_{2n} = 1 - \sum_{m=0}^{2n} \left[\frac{\left(b^{kj} r_{ij}\right)^m}{m!} \right] \mathrm{e}^{-b_{kj} r_{ij}}. \tag{2}$$

The role of these damping functions is to avoid divergence of the dispersion interaction at short distance where the wavefunctions of the two species overlap (i.e. when the interacting species are in contact) [28]. They allow us to take into account the possible electronic exchange which has a non-zero probability at short distance even for two closed shell structures. For each pair of interacting species, they are parametrized with the single b_{kj} repulsive parameter. The damped dispersion multipolar expansion can be seen as a convenient way to make the perturbation theory valid at short inter-atomic separations. The last term in equation (1) is the induction interaction as written in the context of the quantum mechanical perturbation theory applied to intermolecular forces [27]. It represents an attractive energy arising from the coupling of the polarizable electronic cloud of the adsorbate atom of polarizability α_k at position i with the electric field E_i induced by the charges carried by framework species (O, Si and H) that result from the bonding process within the inorganic matrix itself. In the case of water interacting with Vycor, one has to parametrize six different adsorbate/adsorbent-species potentials; all atomic parameters and coefficients are given in tables 1 and 2. Note that repulsive parameters for like pairs are taken from a previous work on the simulation of rare gases in silicalite [25] using Bohm and Ahlrichs [29] combination rules based on *ab initio* results at the Hartree–Fock level approximation which only describes the repulsive energy term in the case of non-charged and polar species. This type of potential function based on the PN-TrAZ parametrization method was used in various studies of molecular and covalent fluids at interfaces from open surfaces [30, 31] to microporous zeolites [32–36] and more recently in the case of mesoporous Vycor-like materials [20, 37, 38, 31, 39–41].

The minimal image convention is adopted to calculate all interactions. The long range mean-field correction to dispersion terms cannot be precisely calculated because the density is not uniform. Actually, the size of the box is large enough (107 Å) that large distance contributions are negligible. The electrostatic contribution is evaluated by summing over neutral subgroups of atoms of highest symmetry (tetrahedral silicon SiO_4 and surface hydroxyls OH). Implementation of the Ewald summation procedure [42] has proven to give little improvement, probably due to the large box size, absence of isolated charges and negligible total dipolar moment of the substrate (due to isotropy in normal orientation on the Vycor surface).

Table 1. PN-TrAZ parameters for water and Vycor species. (Note: $a_0 = 0.529\,177$ Å, $1E_h = 3.1578 \times 10^5$ K.)

	Water		Vycor		
Atoms	Ow	Hw	Si	O	H
q (e)	−0.82	0.41	+2	−1	+0.5
A (E_h)	247.7	1.338	6163.4	1543.5	1.338
b (a_0^{-1})	2.075	2.11	2.395	2.19	2.11
Polarizabilities (a_0^3)	7.56	2.655	2.36	8.03	2.25
N_{eff}	4.476	0.414	1.52	4.656	0.324

Table 2. Dispersion and repulsion parameters obtained in the framework of the PN-TrAZ model with Bohm and Ahlrichs combination rules for repulsive interactions.

Water species	Silica species	C_6 ($E_h a_0^6$)	C_8 ($E_h a_0^8$)	C_{10} ($E_h a_0^{10}$)	A (E_h)	b (a_0^{-1})
Hw	O	8.3157	151.22	2668.6	45.444	2.149
Hw	Si	2.4874	32.919	—	90.811	2.243
Hw	H	1.7340	22.983	—	1.338	2.11
Ow	O	34.850	735.319	13 540.4	618.3	2.131
Ow	Si	10.513	172.72	—	1235.5	2.223
Ow	H	6.4843	116.27	—	18.2	2.092

Calculations show that the largest part of the substrate contribution to electrostatics comes from the surface dipoles (hydroxyls), the tetrahedral SiO_4 giving rise to a weak quadrupolar term only.

In order to save computing time, the water/substrate interactions have been calculated in advance and saved on a grid. This is possible since the substrate is kept rigid in this study. The grid mesh has been chosen equal to 1 Å. Due to the memory constraint it could not be made smaller. However, close to the silica surface, this mesh is not fine enough for a small dipolar molecule such as water. This is why the contribution of the substrate has been divided in two parts, inside and outside a sphere of 6.5 Å in radius, centred on the grid cell to be evaluated. Only the contribution from outside is saved on the grid, the rest being calculated directly during the course of the simulation. A neutrality constraint has been added so as to avoid fast oscillations of electrostatic contributions due to isolated charges coming in and out of the 6.5 Å radius sphere: for instance, O and H atoms from the same surface hydroxyl group are taken together. The choice of the radius is a compromise between CPU time saving and grid smoothness. Three different grids are necessary: two dispersion–repulsion grids for both O and H atoms of water, plus one for electrostatic potential. Since there are eight corners for each cubic cell, and since the 6.5 Å radius sphere has to be centred on the cell, the total number of grids used is 8×3, and interpolation in each cell is made between eight grids. All grids are defined everywhere in the simulation box due to the short distance cut-off. The result obtained with this method for the whole interaction is always within 4% of the value obtained by a completely direct calculation with all the atoms of the simulation box. Our method is then very accurate, and very fast (a few tens of atoms taken into account instead of the 60 000 species that are present in the silica texture of our Vycor numerical sample). This procedure is well suited to study adsorption properties of polar molecules and allows consideration of large systems.

The water–water interaction calculations become excessively slow at low temperature when the substrate is almost completely filled (more than 10 000 water molecules). It was

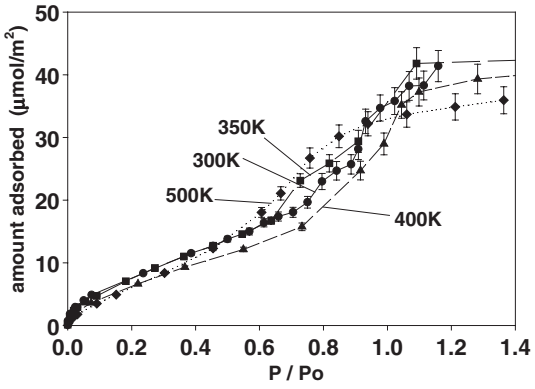

Figure 3. Adsorption isotherms of water in Vycor at various temperatures.

Table 3. SPC water thermodynamic quantities at different temperatures: P^*, bulk saturating vapour pressure [45, 46]; L, bulk latent heat [45, 46]; q_{st}, isosteric heat of adsorption on Vycor; n_0, monolayer capacity; C, parameter, and $\varepsilon - L$, see text.

	300 K	350 K	400 K	500 K
P^*	4.8×10^{-2}	0.52	3	33
L (kJ mol^{-1})	45	41.4	37.8	30.6
q_{st} (kJ mol^{-1})	80	76	70	65
n_0 (μmol m^{-2})	7.47	7.74	6.7	3.3
C	19.3	13.5	12.5	1.55
$\varepsilon - L$ (kJ mol^{-1})	7.38	7.57	8.4	1.8

therefore decided to implement a hierarchy method [43]. The simulation box is divided into a three-dimensional array of 5 Å wide cells. The total interaction energy of a water molecule with the others is the sum of the individual contributions of the molecules contained in the neighbouring cells (within a distance of 15 Å) and the multipole representation for the other cells. The uncertainty introduced by this method does not exceed a few per cent.

4. Water adsorption isotherms

The water adsorption isotherms have been calculated using the grand canonical Monte Carlo simulation [44] (GCMC), which mimics a real adsorption experiment where the temperature, the volume and the chemical potential (related to the pressure of the gas) are kept constant. An equal number of translations, rotations, creations or destructions of molecules has been chosen, around 2×10^4 per water molecule at full saturation, up to 10^5 at low coverage. The isotherms have been calculated for four different temperatures, 300, 350, 400 and 500 K. For each temperature, the pressure of the vapour in the particle reservoir is normalized to the saturating vapour pressure for the SPC model [45, 46] given in table 3. The adsorbed quantity is normalized to the known geometric surface of the numerical sample (401 nm^2) [37], and expressed in μmol m^{-2}. The result is shown in figure 3. As can be seen, the isotherms show strong adsorption at low pressure as expected for hydrophilic surfaces. Above a relative pressure of 0.7 the adsorption increases faster: this is the so-called capillary condensation. However, as can be noted, the full saturation is generally reached above the saturating vapour pressure. This point will be discussed later.

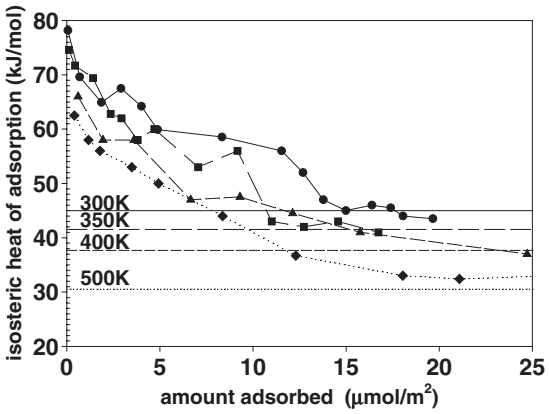

Figure 4. Isosteric heat of adsorption at various temperatures.

The energetics of the adsorption has been analysed by calculating the isosteric heat of adsorption q_{st} on the silica substrate from cross-fluctuations in energy (U) and adsorbed quantity (N) according to the formula [44]

$$q_{st} = -\frac{\langle UN\rangle - \langle U\rangle\langle N\rangle}{\langle N^2\rangle - \langle N\rangle^2} + RT. \tag{3}$$

The values for the four temperatures are given as a function of amount of water adsorbed in figure 4. The bulk SPC water latent heat [46] corresponding to each temperature is also represented as a horizontal line (see table 3). As can be seen for all temperatures the heat of adsorption is significantly higher than the latent heat, which is characteristic of a hydrophilic surface. The initial heat of adsorption obtained for very low pressure reaches 80 kJ mol^{-1} at 300 K, which is 1.8 times the bulk latent heat of water, and 65 kJ mol^{-1} at 500 K, which is 2.1 times the latent heat of water at the same temperature. These values are in agreement with experimental determinations [47], which validate the intermolecular potential used in this work. Inspection shows that the isosteric heat of adsorption has reached its bulk value as soon as the monolayer coverage is reached (around 16 μmol m^{-2} at 300 K). The second layer and subsequent ones are then expected to have properties very similar to the bulk. Furthermore, it can be inferred from these data that the sites are energetically heterogeneous. This point will be reconsidered during the BET analysis.

The Brunauer, Emmett and Teller (BET) [48, 1, 2] model has been applied to the water adsorption isotherms previously calculated to evaluate the monolayer coverage and energetics of the system. In this model the first layer adsorption is supposed to take place on energetically uniform substrate sites with an energy ε close to the heat of adsorption, and the next layers are adsorbed on the previous ones with a different energy, L (supposedly closer to the latent heat of the bulk fluid). Assuming this hypothesis, it is shown that the adsorbed amount n (for instance in μmol m^{-2}) and the relative pressure P/P_0 can be cast in the following equation:

$$\frac{P/P_0}{n(1-P/P_0)} = \frac{1}{n_0 C} + \frac{C-1}{n_0 C} P/P_0 \tag{4}$$

where n_0 is the monolayer capacity expressed in the same units as n (μmol m^{-2}), and $C = \mathrm{e}^{(\varepsilon - L)/kT}$ is related to the difference between heat of adsorption on the substrate and bulk latent heat. Figure 5 shows the left-hand side of equation (4) as a function of reduced pressure. As can be seen the curves show a linear portion between relative pressure of 0.1 and 0.4. However, the low pressure adsorption does not follow the BET model. This was

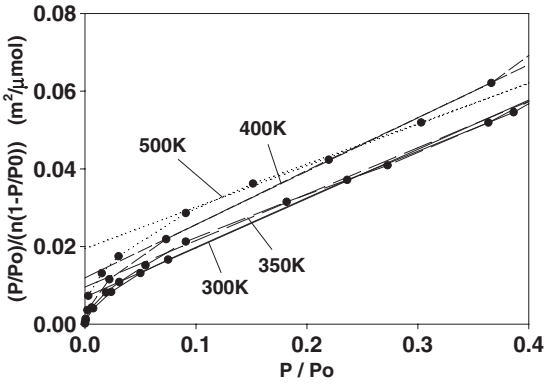

Figure 5. BET plots for water adsorbed in Vycor at various temperatures.

expected since the isosteric heat of adsorption does not show a sharp variation between low pressure, where it is close to the adsorption site energetics, and higher pressure, where the isosteric heat of adsorption is close to the bulk fluid latent heat. The linear regression of the curves between relative pressures of 0.1 and 0.4 has been determined and drawn in figure 5. Their analysis gives the monolayer capacity n_0 and the difference between adsorption energy and bulk latent heat. The results are summarized in table 3. As can be seen, the monolayer capacities at different temperatures are close to each other, except for the highest temperature, which probably corresponds to conditions for which the localized adsorption assumption at the heart of the BET model is no longer valid. The obtained value for the monolayer capacity is around 7.5 μmol m^{-2}, which corresponds to 22 Å^2 per water molecule. This value is much larger than the commonly admitted surface of 10.5 Å^2 per molecule deduced from bulk water density, or even more refined and larger values proposed by different authors (12.5 Å^2 [49], or 14.8 Å^2 [50, 51]), to account for the low specific surface area obtained by BET analysis of water isotherms. Inspection of water configurations shows that the water molecules do not cover the whole surface as already observed for xenon in the same Vycor numerical sample [52]. As a matter of fact, the molecules form disconnected patches of different sizes, leaving some regions completely dehydrated (less hydrophilic sites). The BET surface is a thermodynamic surface in the sense that it is a determination of the area of substrate presenting energetically favourable sites. The previous result has then to be interpreted in terms of heterogeneity of the silica surface, with hydrophilic zones measured by the BET surface and almost as much hydrophobic region not taken into account in the BET surface. This heterogeneity was previously noticed while analysing the isosteric heat of adsorption. It seems then that the BET method for specific surface determination fails to be applicable to our water–silica system. It is proposed that this heterogeneity might explain the relative underestimation of the amount of water that should be adsorbed compared to experiments [47]. The presence of hydrophobic sites also induces a delay in capillary condensation which ends slightly above the saturating vapour pressure. This issue will be reconsidered while analysing the water monolayer structure.

5. Structure analysis

The structure of water adsorbed on Vycor has been analysed in terms of site–site radial distribution functions. The data have been averaged in the grand canonical ensemble, which is expected to give results identical to micro-canonical ensemble molecular dynamics. The site–site radial distribution function has been carefully normalized by taking into account the

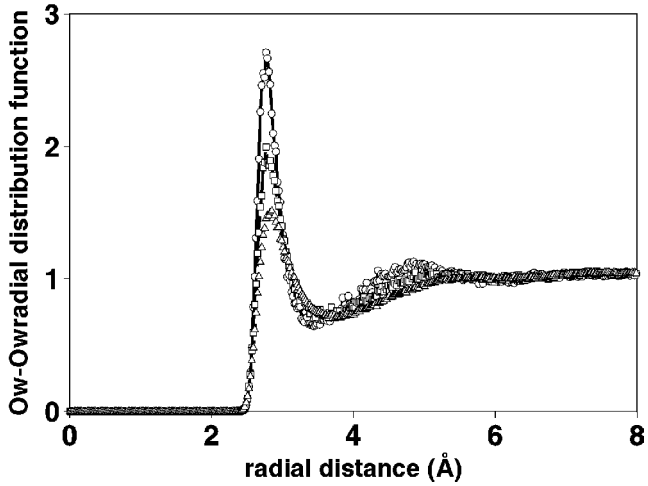

Figure 6. Water oxygen–oxygen pair correlation function $g(r)$: at 300 K (circles), 400 K (squares) and 500 K (triangles).

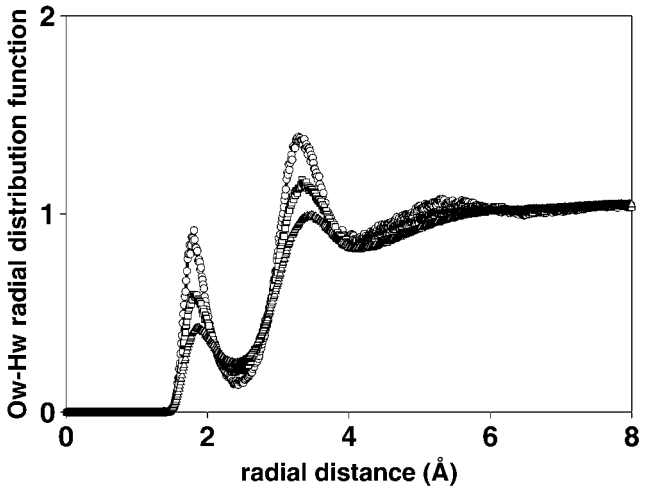

Figure 7. Water oxygen–hydrogen pair correlation function $g(r)$: at 300 K (circles), 400 K (squares) and 500 K (triangles).

excluded volume effect [16]. In this structure analysis, we only consider the adsorbed film on the pore surface. Previous work has already focused on the filling effect, showing strong structure distortion compared to bulk only for monolayer coverage. Actually, the structure of water is expected to be very close to bulk for multilayer coverage. In this analysis, the adsorbed film is supposed to be completed at 15 μmol m^{-2}, which corresponds, by visual inspection to a nearly uniform coverage of the internal surface of Vycor. This corresponds to a relative pressure of about 0.6. However, the higher the temperature, the more diffuse the layer, which is actually not so well defined at 500 K.

The oxygen–oxygen, oxygen–hydrogen and hydrogen–hydrogen radial distribution functions are given for three different temperatures in figures 6–8. Inspection shows that

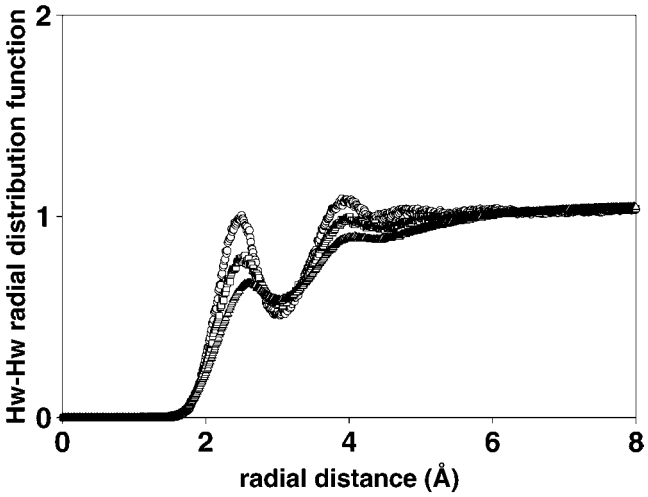

Figure 8. Water hydrogen–hydrogen pair correlation function $g(r)$: at 300 K (circles), 400 K (squares) and 500 K (triangles).

the O–O first peak is situated around 2.8 Å, as for bulk water. The position of the maximum is slightly shifted to larger values as the temperature increases, as expected. The larger the temperature the broader the peak, due to thermal agitation. The second peak is situated around 5 Å, slightly displaced compared to the bulk (4.5 Å). It corresponds to the formation of chains of water molecules each having two neighbours. Such a displacement was first observed by Brovchenko *et al* [53, 54] and also reported by Gallo *et al* [11]. Furthermore it has been shown [54] that the intensity of this displaced second peak depends on the strength of the water–substrate interaction. The more intense the interaction, the stronger the peak. This suggests that the second peak at 5 Å is related to the quasi-bi-dimensional character of the adsorbed film. For temperatures above 400 K, this second peak disappears. The O–H correlation function also shows well defined peaks at positions close to bulk values. By contrast, peak intensities are lower for confined water. As for the O–O correlation function, the peaks decrease, broaden and shift to larger distances as the temperature increases. The third peak disappears above 400 K due to thermal agitation. The same remarks hold true for the H–H radial distribution function. In a neutron scattering experiment, the total site–site correlation function is a weighted sum of the partial atom–atom correlation functions (according to the atomic cross-sections). Since the hydrogen cross-section is unfavourable, the hydrogen species are generally replaced by deuterium in a real experiment, and in this case the total correlation function is written as [55]

$$l(r) = 0.489 g_{\mathrm{O-O}}(r) + 0.421 g_{\mathrm{O-D}}(r) + 0.090 g_{\mathrm{D-D}}(r). \tag{5}$$

This quantity is shown in figure 9. At 500 K the total correlation function shows only two peaks at 1.87 and 2.88 Å. They correspond to the O–H and O–O first peak contributions. When the temperature decreases, a third peak appears around 5 Å, from O–O position correlations. Inspection also shows the appearance of a shoulder at 3.3 Å, which corresponds to the second peak of the O–H correlation function.

To get more insight into the water–silica interaction, the site–site correlation functions have been calculated between the two species of surface hydroxyl (O and H of Vycor, written as Ov and Hv), and water species (written as Ow and Hw, for water). The Ov–Ow radial distribution functions for different temperatures are given in figure 10. The curves present a broad pronounced peak around 3.3 Å, and another one around 4.5 Å. The lower the temperature,

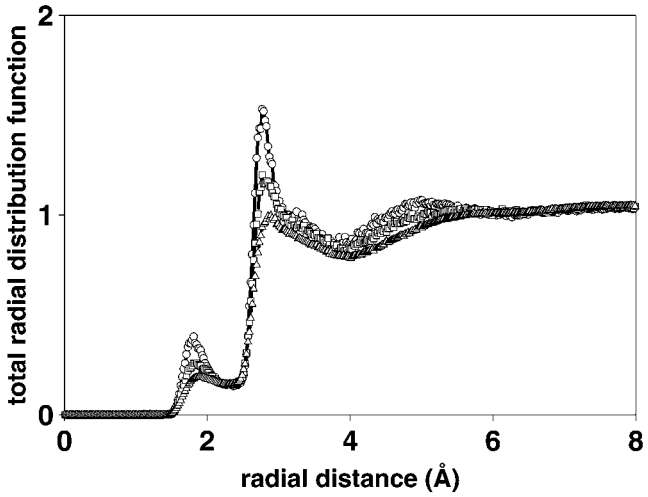

Figure 9. Total water–water $l(r)$ (see text).

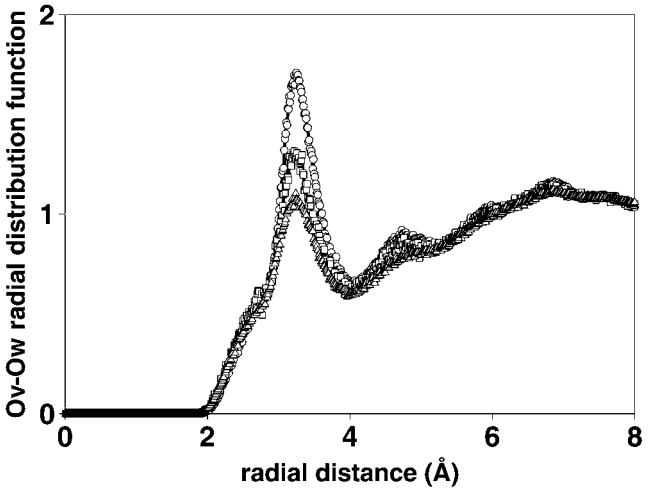

Figure 10. Water oxygen–Vycor oxygen pair correlation function $g(r)$: at 300 K (circles), 400 K (squares) and 500 K (triangles).

the more defined the peak. At low temperature (300 K), a shoulder appears at 2.7 Å. The comparison with the water–water O–O radial distribution function shows strong differences. The main correlation between the oxygen species of water (at 2.8 Å) is broadened and displaced to larger distances (3.3 Å), whereas a shoulder appears at 2.7 Å (as the temperature decreases). It shows that the surface hydroxyls are not implied in the water tetrahedral structure in the same way as water molecules. However, the second peak, visible for temperatures lower than 400 K, is not much affected. The O–H correlation functions shown in figures 11 and 12 are strongly distorted compared to the bulk. As the temperature decreases, a main peak appears around 2.8 Å instead of two in bulk water. This means that the dissymmetry of the distances between on one hand the oxygen of one molecule and hydrogen of the other and on the other hand the hydrogen of the first molecule and the oxygen of the second tends to disappear. The locally

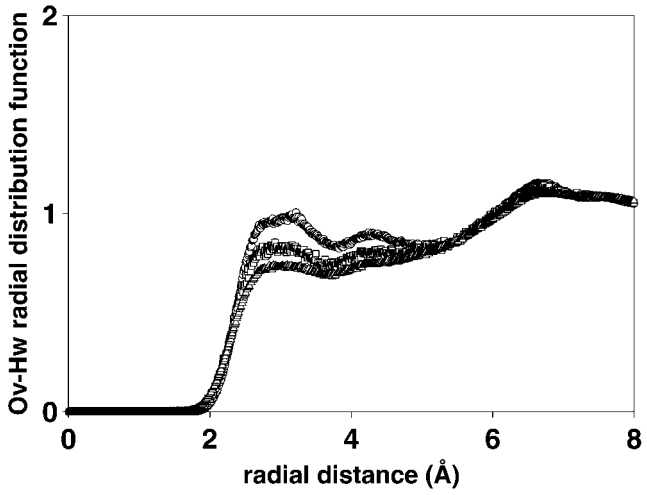

Figure 11. Water hydrogen–Vycor oxygen pair correlation function $g(r)$: at 300 K (circles), 400 K (squares) and 500 K (triangles).

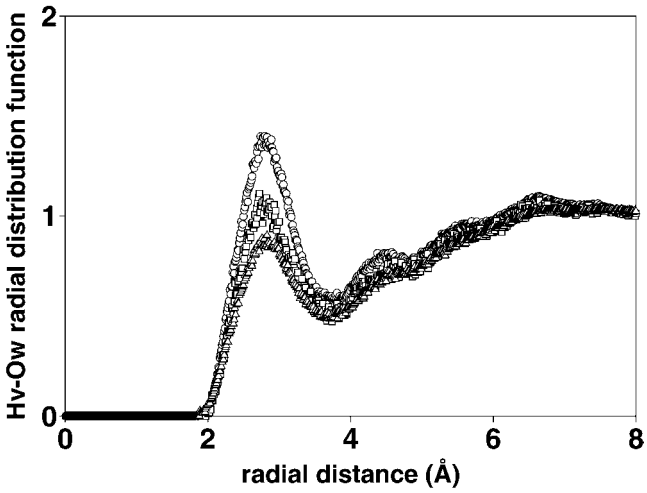

Figure 12. Water oxygen–Vycor hydrogen pair correlation function $g(r)$: at 300 K (circles), 400 K (squares) and 500 K (triangles).

tetrahedral structure of water is broken, probably due to the fact that the surface hydroxyls have their dipole moment parallel to the O–H axis, whereas for a water molecule the dipole moment is not parallel to any of the O–H directions. The H–H correlations (see figure 13) show, for low temperature, a broad peak around 2.6 Å and a small one around 4.4 Å. These peaks are reminiscent of the first and third peaks in bulk water positioned at 2.4 and 4.6 Å respectively. It is expected that the second peak at 3.8 Å in bulk water will be absent because the surface hydroxyls contain only one hydrogen. These data then imply that the H–H average distance is larger than in bulk. In conclusion, it seems that the hydrogen bond is elongated, and might not meet the energetic criterion stating that a hydrogen bond has a characteristic energy around 10 kJ mol^{-1} (analysis underway). These strong structural modifications might be understood

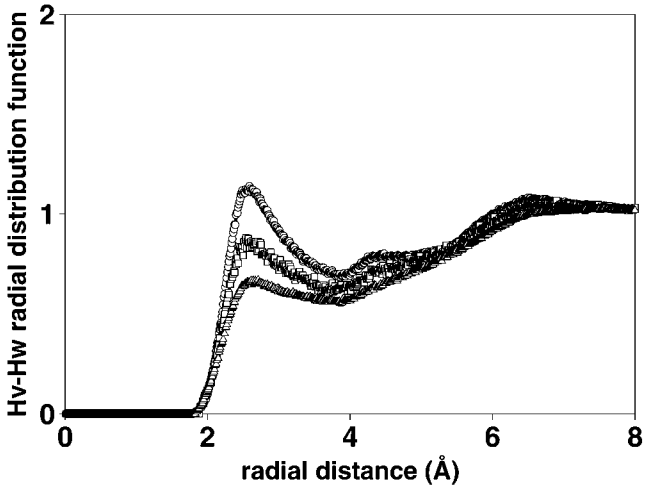

Figure 13. Water hydrogen–Vycor hydrogen pair correlation function $g(r)$: at 300 K (circles), 400 K (squares) and 500 K (triangles).

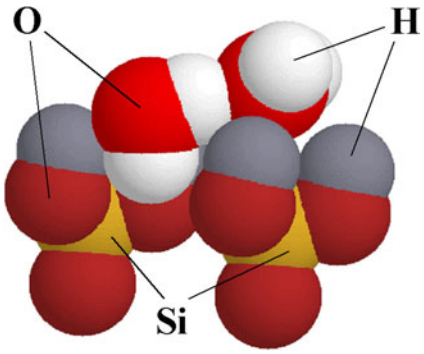

Figure 14. Molecular configuration showing two water molecules adsorbed on a portion of silica surface.

(This figure is in colour only in the electronic version)

by considering that the electric field in the vicinity of the surface hydroxyls differs significantly from that of a water molecule. For instance, the dipole moment of the hydroxyls is directed along the O–H direction, which is not the case for water. The partial charges carried by the oxygen and hydrogen species are not identical (see table 1). Furthermore, the silicon tetrahedron gives rise to a quadrupole moment in the vicinity of the silica surface. Figure 14 shows a molecular configuration of water adsorbed on the silica surface. Only two tetrahedral SiO_4 are represented for clarity, and two adsorbed molecules. Inspection shows that the water molecules and surface hydroxyls are not inserted in a tetrahedral structure as mentioned before.

6. Conclusion

A thermodynamic and structure analysis of the water–silica system at the mesoporous scale has been carried out in the grand canonical ensemble using a grand canonical Monte Carlo

simulation. The numerical mesoporous glass has been obtained by an off-lattice reconstruction method. It reproduces quite well the geometric complexity of real Vycor, such as its specific surface area, pore size, chord distribution and correlation peak in small angle neutron scattering spectra. Its surface chemistry is made realistic by hydroxylating the surface. The adsorbed water is described by the SPC model, and water–silica interactions are calculated in the framework of the PN-TrAZ model. The thermodynamic quantities such as water adsorption isotherms and isosteric heat of adsorption have been calculated for different temperatures. The model has proven to reproduce quite well the first steps of water adsorption. Since the geometric surface is known, the BET analysis allows us to calculate the monolayer capacity, or the inverse, which is the mean surface occupied by a single water molecule of the monolayer. The value obtained (22 $Å^2$) is significantly larger than the value deduced from bulk water density (10.5 $Å^2$). It is qualitatively in agreement with experimental observations. On the other hand, the structure of the adsorbed film prior to capillary condensation has been studied in the same statistical ensemble. It shows a strong distortion of the pair correlation functions compared to bulk water due to the influence of the silica surface. The hydrogen bond is significantly elongated, and angles distorted. In a further study the surface hydroxyls will be made free to rotate, which was not the case in this work for the sake of simplicity. However, it is thought that this will probably greatly influence the monolayer structure, which might re-accommodate some bulk water features.

Acknowledgment

The Institut de Développement des Ressources en Informatique Scientifique (IDRIS-CNRS, Orsay, France) is gratefully acknowledged for the CPU grant no 031153.

References

[1] Gregg S J and Sing K S W 1982 *Adsorption, Surface Area and Porosity* (New York: Academic)
[2] Rouquerol F, Rouquerol J and Sing K S W 1999 *Adsorption by Powders and Porous Solids* (London: Academic)
[3] Korb J-P 2001 *Magn. Reson. Imaging* **19** 363
[4] Dore J 2000 *Chem. Phys.* **258** 327
[5] Bellissent-Funel M-C, Longeville S, Zanotti J M and Chen S H 2000 *Phys. Rev. Lett.* **85** 3644
[6] Agamalian M, Drake J M, Sinha S K and Axe J D 1997 *Phys. Rev.* E **55** 3021
[7] Lee S H and Rossky P J 1994 *J. Chem. Phys.* **100** 3334
[8] Spohr E, Trokhymchuk A and Henderson D 1998 *J. Electroanal. Chem.* **450** 281
[9] Rovere M, Ricci M A, Vellati D and Bruni F 1998 *J. Chem. Phys.* **108** 9859
[10] Hartnig C, Witschel W, Spohr E, Gallo P, Ricci M A and Rovere M 2000 *J. Mol. Liq.* **85** 127
[11] Gallo P, Ricci M A and Rovere M 2002 *J. Chem. Phys.* **116** 342
[12] Hansen E W, Schmidt R, Stöcker M and Akporiaye D 1995 *J. Phys. Chem.* **99** 4148
[13] Takahara S, Nakano M, Kittaka S, Kuroda Y, Mori T, Hamano H and Yamaguchi T 1999 *J. Phys. Chem.* B **103** 5814
[14] Bellissent-Funel M-C, Lal J and Bosio L 1993 *J. Chem. Phys.* **98** 4246
[15] Bruni F, Ricci M A and Soper A K 1998 *J. Chem. Phys.* **109** 1478
[16] Soper A K, Bruni F and Ricci M A 1998 *J. Chem. Phys.* **109** 1486
[17] Levitz P E 1998 *Adv. Colloid Interface Sci.* **76/77** 71
[18] Levitz P, Ehret G, Sinha S K and Drake J M 1991 *J. Chem. Phys.* **95** 6151
[19] Levitz P E and Tchoubar D 1992 *J. Physique* I **2** 771
[20] Pellenq R J-M, Rousseau B and Levitz P E 2001 *Phys. Chem. Chem. Phys.* **3** 1207
[21] Landmesser H, Kosslick H, Storek W and Frick R 1997 *Solid State Ion.* **101–103** 271
[22] Low M J D and Ramasubramanian N 1967 *J. Phys. Chem* **71** 730
[23] Berendsen H J C, Postma J P M, van Gunsteren W F and Hermans J 1981 *Intermolecular Forces* ed B Pullman (Dordrecht: Reidel) p 331
[24] Jorgensen W L, Chandrasekhar J, Madura J D, Impey R W and Klein M L 1983 *J. Chem. Phys.* **79** 926

[25] Pellenq R J-M and Nicholson D 1994 *J. Phys. Chem.* **98** 13339
[26] Pellenq R J-M and Nicholson D 1998 *Mol. Phys.* **95** 549
[27] Stone A 1996 *The Theory of Intermolecular Forces* (Oxford: Clarendon)
[28] Tang K T and Toennies J P 1984 *J. Chem. Phys.* **80** 3726
[29] Bohm H J and Ahlrichs R 1982 *J. Chem. Phys.* **77** 2028
[30] Marinelli F, Grillet Y and Pellenq R J-M 1999 *Mol. Phys.* **97** 1207
[31] Puibasset J and Pellenq R J-M 2003 *J. Chem. Phys.* **118** 5613
[32] Lachet V, Boutin A, Tavitian B and Fuchs A H 1998 *J. Phys. Chem.* B **102** 9224
[33] Nicholson D and Pellenq R J-M 1998 *Adv. Colloid Interface Sci.* **76/77** 179
[34] Fuchs A H and Cheetham A K 2001 *J. Phys. Chem.* B **105** 7375
[35] Grey T J, Nicholson D, Gale J D and Peterson B K 2002 *Appl. Surf. Sci.* **196** 105
[36] Bichara C, Yves-Raty J and Pellenq R J-M 2002 *Phys. Rev. Lett.* **89** 016101
[37] Pellenq R J-M and Levitz P E 2002 *Mol. Phys.* **100** 2059
[38] Puibasset J and Pellenq R J-M 2002 *Proc. 6th Int. Symp. on the Characterization of Porous Solids (Alicante, Spain, May 2002)* (*Studies in Surface Science and Catalysis* vol 144) ed F Rodriguez Reinoso, B McEnaney, J Rouquerol and K Unger (Amsterdam: Elsevier) p 371
[39] Puibasset J and Pellenq R J-M 2003 *J. Chem. Phys.* **119** 9226
[40] Puibasset J and Pellenq R J-M 2003 *Eur. Phys. J.* E **12** 017
[41] Coasne B and Pellenq R J-M 2004 *J. Chem. Phys.* **120** 2913
[42] Ewald P 1921 *Ann. Phys.* **64** 253
Heyes D M 1994 *Phys. Rev.* B **49** 755
[43] Ding H-Q, Karasawa N and Goddard W A III 1992 *J. Chem. Phys.* **97** 4309
[44] Nicholson D and Parsonage N G 1982 *Computer Simulation and the Statistical Mechanics of Adsorption* (London: Academic)
[45] Errington J R and Panagiotopoulos A Z 1998 *J. Phys. Chem.* B **102** 7470
[46] Vorholz J, Harismiadis V I, Rumpf B, Panagiotopoulos A Z and Maurer G 2000 *Fluid Phase Equilib.* **170** 203
[47] Takei T, Yamazaki A, Watanabe T and Chikazawa M 1997 *J. Colloid Interface Sci.* **188** 409
[48] Brunauer S, Emmett P H and Teller E 1938 *J. Am. Chem. Soc.* **73** 373
[49] Staszczuk P, Jaroniec M and Gilpin R K 1996 *Thermochim. Acta* **287** 225
[50] Cases J M, Berend I, Delon J F, François M, Grillet Y, Michot L, Poirier J E and Yvon J 1990 *Matériaux Argileux* ed A Decarreau (Paris: Soc. Fr. Miner. and Crist.) p 309
[51] Legrand A P 1998 *The Surface Properties of Silicas* (Chichester: Wiley) p 33
[52] Pellenq R J-M, Rodts S, Pasquier V, Delville A and Levitz P E 2000 *Adsorption* **6** 241
[53] Brovchenko I, Paschek D and Geiger A 2000 *J. Chem. Phys.* **113** 5026
[54] Brovchenko I and Geiger A 2002 *J. Mol. Liq.* **96/97** 195
[55] Soper A K and Phillips M G 1986 *Chem. Phys.* **107** 47